Journal of Power Sources 195 (2010) 6420–6427

Contents lists available at ScienceDirect

Journal of Power Sources

journal homepage: www.elsevier.com/locate/jpowsour

# Effect of unsintered gadolinium-doped ceria buffer layer on performance of metal-supported solid oxide fuel cells using unsintered barium strontium cobalt ferrite cathode

Yu-Mi Kim [a], Pattaraporn Kim-Lohsoontorn [b,c], Joongmyeon Bae [a,c,*]

[a] Department of Mechanical Engineering, Korea Advanced Institute of Science and Technology (KAIST), Daejeon 305-701, Republic of Korea
[b] Department of Chemical Engineering, Mahidol University, Nakorn Pathom 73170, Thailand
[c] KI for Eco-Energy, Korea Advanced Institute of Science and Technology (KAIST), Daejeon 305-701, Republic of Korea

ARTICLE INFO

*Article history:*
Received 2 March 2010
Received in revised form 15 March 2010
Accepted 22 March 2010
Available online 3 April 2010

*Keywords:*
Buffer layer
Unsintered buffer layer
Unsintered cathode
Metal-supported solid oxide fuel cell
Barium strontium cobalt ferrite
Gadolinium-doped ceria

ABSTRACT

In this study, a $Gd_{0.1}Ce_{0.9}O_{1.95}$ (GDC) buffer layer and a $Ba_{0.5}Sr_{0.5}Co_{0.8}Fe_{0.2}O_{3-\delta}$ (BSCF) cathode, fabricated without pre-sintering, are investigated (unsintered GDC and unsintered BSCF). The effect of the unsintered GDC buffer layer, including the thickness of the layer, on the performance of solid oxide fuel cells (SOFCs) using an unsintered BSCF cathode is studied. The maximum power density of the metal-supported SOFC using an unsintered BSCF cathode without a buffer layer is 0.81 W cm$^{-2}$, which is measured after 2 h of operation (97% $H_2$ and 3% $H_2O$ at the anode and ambient air at the cathode), and it significantly decreases to 0.63 W cm$^{-2}$ after 50 h. At a relatively low temperature of 800 °C, $SrZrO_3$ and $BaZrO_3$, arising from interaction between BSCF and yttria-stabilized zirconia (YSZ), are detected after 50 h. Introducing a GDC interlayer between the cathode and electrolyte significantly increases the durability of the cell performance, supporting over 1000 h of cell usage with an unsintered GDC buffer layer. Comparable performance is obtained from the anode-supported cell when using an unsintered BSCF cathode with an unsintered GDC buffer layer (0.75 W cm$^{-2}$) and sintered GDC buffer layer (0.82 W cm$^{-2}$). When a sintered BSCF cathode is used, however, the performance increases to 1.23 W cm$^{-2}$. The adhesion between the BSCF cathode and the cell can be enhanced by an unsintered GDC buffer layer, but an increase in the layer thickness (1–6 μm) increases the area specific resistance (ASR) of the cell, and the overly thick buffer layer causes delamination of the BSCF cathode. Finally, the maximum power densities of the metal-supported SOFC using an unsintered BSCF cathode and unsintered GDC buffer layer are 0.78, 0.64, 0.45 and 0.31 W cm$^{-2}$ at 850, 800, 750 and 700 °C, respectively.



## 1. Introduction

The solid oxide fuel cell (SOFC) is a promising energy conversion technology due to its fuel flexibility, high efficiency and ability to deliver high-grade heat and electrical power [1–3]. Considerable advances have been made in the development of metal-supported solid oxide fuel cells (SOFCs) [4–14]. By using a metal support, relatively low-cost materials can be used and this enables easy, cost-effective and large-scale fabrication. In particular, sealing is facilitated because conventional metal-joining techniques, such as welding or brazing, can be used. Metal-supported SOFCs are also readily engineered with high mechanical strength to withstand compacted and/or vibration assembly, which can greatly simplify system requirements.

One challenge facing the development of metal-supported SOFCs is cell fabrication [6,7]. A high sintering temperature (>1000 °C) is needed to increase electrolyte densification, promote adhesion between electrodes and electrolyte, and form well-structured electrodes. Unfortunately, however, sintering at high temperature in ambient air introduces serious metal substrate oxidation. There has been a large body of work dedicated to the study of metal-supported SOFC fabrication. Cells have been fabricated using various techniques, such as pulsed laser deposition and wet ceramic processes at the National Research Council Canada, Canada [8], atmospheric plasma spray processing at Julich, Germany [9], high temperature sintering in a reducing atmosphere at the Lawrence Berkeley National Laboratory, USA [10,11], and vacuum plasma spray processing at the Aerospace Research Center and Space Agency, USA [12–14].

* Corresponding author at: Department of Mechanical Engineering, Korea Advanced Institute of Science and Technology (KAIST), Guseong-Dong, Yuseong-Gu, Daejeon 305-701, Republic of Korea. Tel.: +82 42 350 3045; fax: +82 42 350 3210.
*E-mail address:* jmbae@kaist.ac.kr (J. Bae).

0378-7753/$ – see front matter © 2010 Elsevier B.V. All rights reserved.
doi:10.1016/j.jpowsour.2010.03.095

Previous work [4] has demonstrated the metal–ceramic sheet-joining process, which can be an option for reducing the fabrication costs of metal-supported SOFCs. Metal substrates and ceramic sheets (comprising the anode and electrolyte layers) were combined using an adhesive paste. After sintering under a reducing atmosphere (composed of 4% $H_2$ and 96% He) to promote good adhesion between the substrate and the ceramic sheet, a cathode was deposited. This assembly was then further subjected to heat treatment. It was found that sintering the cathode at 1273 K in air caused oxidation of the metal substrate which, in turn, led to a significant degradation of cell performance. Unfortunately, sintering of the cathode in a reducing atmosphere can cause the development of unstable states and cation precipitation, which lead to reduced cell performance [15]. Moreover, in the case of alkaline earth metal-doped $LaCrO_3$ materials, it has been reported that sintering the cathode in an inert atmosphere can cause microstructural cracks and phase changes [16]. To overcome this problem, a cathode that is capable of acceptable performance without undergoing a pre-sintering process is required. Throughout this work, buffer layers and cathodes prepared without the benefit of a pre-sintering process will be referred to as 'unsintered buffer layers' and 'unsintered cathodes', respectively. Recently, it is found that an unsintered $Ba_{0.5}Sr_{0.5}Co_{0.8}Fe_{0.2}O_{3-\delta}$ (BSCF) cathode can be a promising option for SOFCs operated at 1073 K. The unsintered BSCF exhibited a greater sinterability at relatively low temperatures compared with unsintered $La_{0.8}Sr_{0.2}MnO_{3-\delta}$ (LSM) and unsintered $La_{0.6}Sr_{0.4}Co_{0.8}Fe_{0.2}O_{3-\delta}$ (LSCF) [17].

The cobalt-based cathodes, including BSCF, are not compatible with yttria-stabilized zirconia (YSZ), as they produce interfacial-insulating layers during high temperature sintering, which leads to a degradation in cell performance [18,19]. It is known, however, that $CeO_2$ is compatible with YSZ. Therefore, this ceria-based material was used as a buffer layer between the cathode and electrolyte [20], or was employed as the electrolyte in place of YSZ [21]. In this study, $Gd_{0.1}Ce_{0.9}O_{1.95}$ (GDC) is used as a buffer layer situated between an unsintered BSCF cathode and YSZ electrolyte. A ceria-based electrolyte like GDC does not exhibit phase stability in reducing atmospheres at high temperatures [22]. Similar to the unsintered BSCF cathode, the GDC-buffered cell cannot be sintered under reducing conditions. Therefore, the performance and microstructure of a metal-supported cell, having an unsintered GDC buffer layer and unsintered BSCF cathode, are investigated.

In this study, BSCF powder was synthesized using a glycine nitrate process. The performance of cells with and without an unsintered buffer layer is investigated, together with the chemical compatibility of unsintered BSCF and YSZ under the same operating conditions. The electrochemical performance and microstructure of the cells in the absence and presence of buffer layers are compared. The performance of cells having GDC buffer layers fabricated with and without a pre-sintering process is also examined. The effect of the thickness of the GDC buffer is also evaluated.

## 2. Experimental

### 2.1. Preparation of BSCF powder and cathode paste

BSCF ($Ba_{0.5}Sr_{0.5}Co_{0.8}Fe_{0.2}O_{3-\delta}$) powders were prepared by the glycine nitrate process (GNP) [23]. Appropriate amounts of $Ba(NO_3)_2$, $Sr(NO_3)_2$, $Co(NO_3)\cdot 6H_2O$ and $Fe(NO_3)_3\cdot 9H_2O$ powders (Alfa Aesar, USA) were initially dissolved with glycine ($C_2H_5NO_2$) (Sigma Aldrich, USA) in deionized water. The solution was then heated until it ignited. The ignited powder was calcined in air at 1000 °C for 8 h and then ball-milled for 24 h in ethanol. After removing the ethanol by baking at 100 °C for 24 h, the BSCF powder was dispersed in a combination of 20 wt.% α-terpineol (Sigma Aldrich, USA) and 80 wt.% cellulose (Sigma Aldrich, USA) to obtain the cathode ink.

**Table 1**
Prepared samples used in this study.

| Cell type | Assembly |
|---|---|
| Metal-supported SOFC | Ni-YSZ\|YSZ\|unsintered BSCF |
| Half-cell | Unsintered BSCF\|YSZ\|unsintered BSCF |
| Half-cell | Unsintered BSCF\|sintered GDC\|YSZ\|sintered GDC\|unsintered BSCF |
| Anode-supported SOFC | Ni-YSZ\|YSZ\|sintered GDC\|unsintered BSCF |
| Anode-supported SOFC | Ni-YSZ\|YSZ\|unsintered GDC\|unsintered BSCF |
| Anode-supported SOFC | Ni-YSZ\|YSZ\|sintered GDC\|sintered BSCF |
| Metal-supported SOFC | Ni-YSZ\|YSZ\|unsintered GDC\|unsintered BSCF |

### 2.2. Preparation of buffer layer paste

The GDC paste was prepared by mixing a commercially available GDC powder (ANAN KASEI, Japan) that had a particle size of 0.5 μm with an organic ink (α-terpineol and ethyl cellulose) at the same composition as for the cathode paste. The weight ratio of organic ink to GDC powder was 0.6.

### 2.3. Cell fabrication

For half-cell tests, an 8 mol% yttria-stabilized zirconia (8YSZ, Tosho, Japan) powder was uniaxially pressed (10 MPa, 60 s), followed by sintering at 1500 °C in air for 4 h to give a dense pellet (~95% calculated density) with a diameter of ~26.0 mm and thickness of ~1.48 mm. A GDC buffer layer was brushed on both sides of the YSZ electrolyte, which was subsequently heat-treated at 100 °C for 30 min in air to create an unsintered GDC buffer layer. After that, the cathode layers were screen-printed on both sides of the buffered pellet and dried at 200 °C for 12 h to remove organic residuals. With no pre-sintering process for the cathode, the cathode layers had a circular area of 0.785 $cm^2$ and a thickness of ~16 μm.

For single-cell tests, both anode-supported and metal-supported SOFCs were fabricated. Studies involving cells with a sintered BSCF cathode and a sintered GDC buffer layer were carried out using anode-supported cells to investigate the effect of the sintered buffer layer and sintered cathode on SOFC performance, while avoiding complications from metal substrate oxidation. The performance of metal-supported SOFCs, fabricated using an unsintered BSCF cathode with/without an unsintered GDC buffer layer was also measured. Fabrication of the single metal-supported SOFCs used in this study was based on a previous report [4]. A summary of the type and assembly of samples prepared in this study is presented in Table 1.

To fabricate the anode-supported cell, NiO powder (J.T. Baker, USA) and 8YSZ powder were mixed in a weight ratio of 60:40 and ball-milled for 24 h using ethanol as the media. Twelve weight percent starch was added as the pore former to create sufficient porosity in the anode. The mixed powder was pressed into a pellet, followed by sintering at 1200 °C for 2 h to give a pellet with a diameter of ~26.0 mm and a thickness of ~1.05 mm. The YSZ slurry was blended with 15 wt.% binder (butvar B-98, Sigma Aldrich), 2 wt.% dispersant (polyvinylpyrrolidone, Sigma Aldrich) and 10 wt.% plasticizer (polyethyleneglycol, Sigma Aldrich). The YSZ slurry was then ball-milled for 36 h. A dip-coating technique was used to deposit a YSZ electrolyte layer, followed by sintering of the YSZ-dipped anode at 1500 °C for 4 h. In the case of the unsintered buffer layer, the GDC layer was fabricated using the same method as that used in the half-cell. For the study of GDC thickness, GDC brushing was repeated after drying to form various thicknesses. In the case of the

sintered buffer layer, the GDC layer was sintered at 1300 °C for 4 h. It should be noted that the large sintering temperature gap between the YSZ electrolyte (~1500 °C) and cathode (~1000 °C) can result in an inferior interface and may reduce triple-phase boundaries. Thus, GDC buffer layers are generally sintered in the temperature range of 1100–1350 °C [24]. The area of the buffer layer was about 1.45 $cm^2$. The cathode ink was screen-printed on the buffered pellet, which was dried at 200 °C for 1 h to give an unsintered cathode layer of 0.785 $cm^2$. In the case of the sintered BSCF, the cell was fired at 1000 °C for 1 h.

### 2.4. Characterization and microstructure measurements

X-ray diffraction (XRD) patterns of the powders were obtained (Rigaku D/MAX IIIC, Japan) using Cu Kα radiation (λ = 1.5428 Å) at 40 kV and 40 mA. The XRD data were collected at 0.01° with a counting time of 1 s per step in the 2θ range from 20° to 80°. The scanning electron microscope (SEM) images of single-cells having unsintered BSCF and GDC buffer layers were taken at 15 kV under a vacuum of $1.5 \times 10^{-5}$ Torr (HITACHI FE-SEM S-4300, Japan).

### 2.5. Electrochemical performance measurements

The *I–V–P* characteristics of single-cells were measured using linear sweep current techniques. A potentiostat/galvanostat operating in galvanostatic mode was used to control the current from 0 to 2.0 A at a scan rate of 0.01 $As^{-1}$. The impedance measurements of half-cells were then performed at open-circuit voltage (OCV) under a potentiostatic mode using a sinusoidal signal amplitude of 20 $mV_{rms}$ over the frequency range of $10^6$–$10^{-2}$ Hz. The electrochemical impedance was collected with a Solartron SI 1287 ECI equipped with a frequency response analyzer (Solartron, SI 1255 FRA, USA).

Electrical connections were made to the cell electrodes via platinum wires and paste (the wire was 0.25 mm in diameter, 99.99% Pt, from Nilaco, Japan), which were put under compression. For half-cell measurements, the cell holder was placed inside a quartz tube, with gas inlet and outlet points, allowing control over the gaseous environment to which the cell was exposed. A tube furnace was used to control the temperature of the test rig. For single-cell measurements, the cell ridge was sealed using sealant (Ultra-temp 516, Aremco, USA) to isolate the gas environments of the two electrodes. The test system allowed a gas composition of $H_2/N_2$ to be introduced into the anode chamber with the total flow rate of 50 sccm, and ambient air was fed to the cathode at 100 sccm. The $H_2/N_2$ line passed through a humidifier, which was a bubble column situated inside a thermocirculator bath, to humidify the flowing gas to the required level (3 mol% humidified $H_2$). The water content in the feed air was removed using a chemical dehumidifier.

## 3. Results and discussion

### 3.1. Performance of metal-supported single-cells with an unsintered BSCF cathode in the absence of a GDC buffer layer

The measurements are initially performed on a cell without a buffer layer between cathode and electrolyte to establish the base response expected from the cell when not being affected by the buffer layer. The *I–V–P* characteristics of a metal-supported single-cell with an unsintered BSCF cathode (Ni-YSZ/YSZ/unsintered BSCF), measured after 2 and 50 h of operation at 800 °C (97% $H_2$ and 3% $H_2O$ to the anode and ambient air to the cathode), is shown in Fig. 1. A maximum power density of 0.81 W $cm^{-2}$ is achieved from the cell after 2 h of operation. Continued operation causes a serious degradation in cell performance. After 50 h of operation, the maximum powder density has decreased to 0.63 W $cm^{-2}$ (degradation rate of 22% per 50 h). It should be noted that degradation rates ranging from 0 to 4.3% per 1000 h have been observed in previous studies of SOFCs [25]. The results show that although not being affected by a high sintering temperature because an unsintered BSCF is used, cell performance degradation still occurs from long-term operation at 800 °C. This degradation can be caused by undesired phases arising from chemical reactions between BSCF and YSZ during the long-term operation.

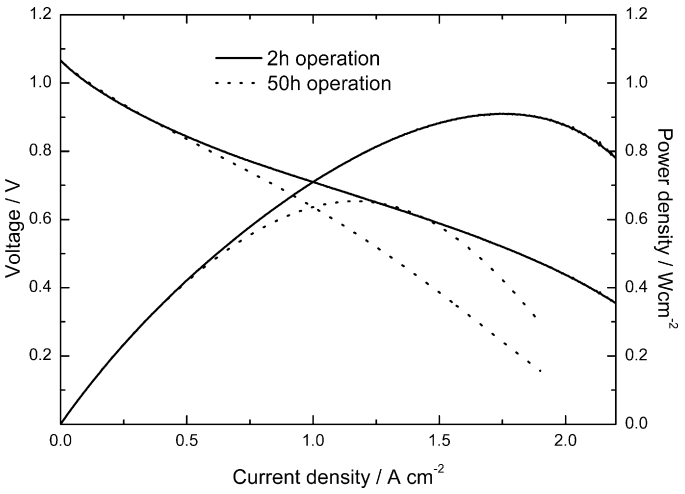


**Fig. 1.** *I–V–P* characteristics after 2 h and 50 h of metal-supported single-cell using unsintered BSCF cathode without GDC buffer layer at 800 °C, with exposure to 97% $H_2$ and 3% $H_2O$ at anode and ambient air at cathode.

The chemical compatibility between BSCF and YSZ at 800 °C was then investigated. BSCF powder and electrolyte powder were mechanically mixed with acetone and $ZrO_2$ media for 24 h and then dried at 100 °C for 24 h. The dried mixed powder was pressed into a pellet (2 MPa, 1 min), followed by firing at 800 °C for 50 h. The pellet was again milled into a powder, and the XRD pattern was measured at room temperature. The XRD patterns of BSCF/YSZ mixed powders, fired at 800 °C for 50 h, are presented in Fig. 2. The XRD peaks for perovskite and fluorite structures, as well as secondary phases such as $SrZrO_3$ and $BaZrO_3$, are detected. The temperature regime in which interaction between BSCF and YSZ occurs has been reported to vary from 850 to 900 °C [26,27]. Duan et al. [26] reported that a firing temperature of 850 °C for 2 h can lead to the formation of secondary phases due to chemical reactions between BSCF and YSZ;

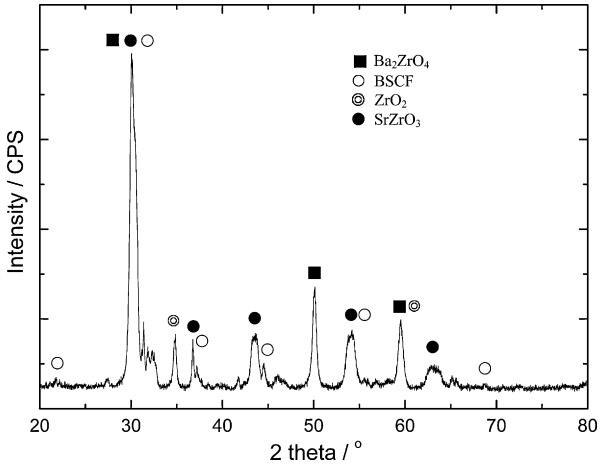


**Fig. 2.** XRD patterns obtained from a mixture of BSCF and YSZ powder fired at 800 °C for 50 h.

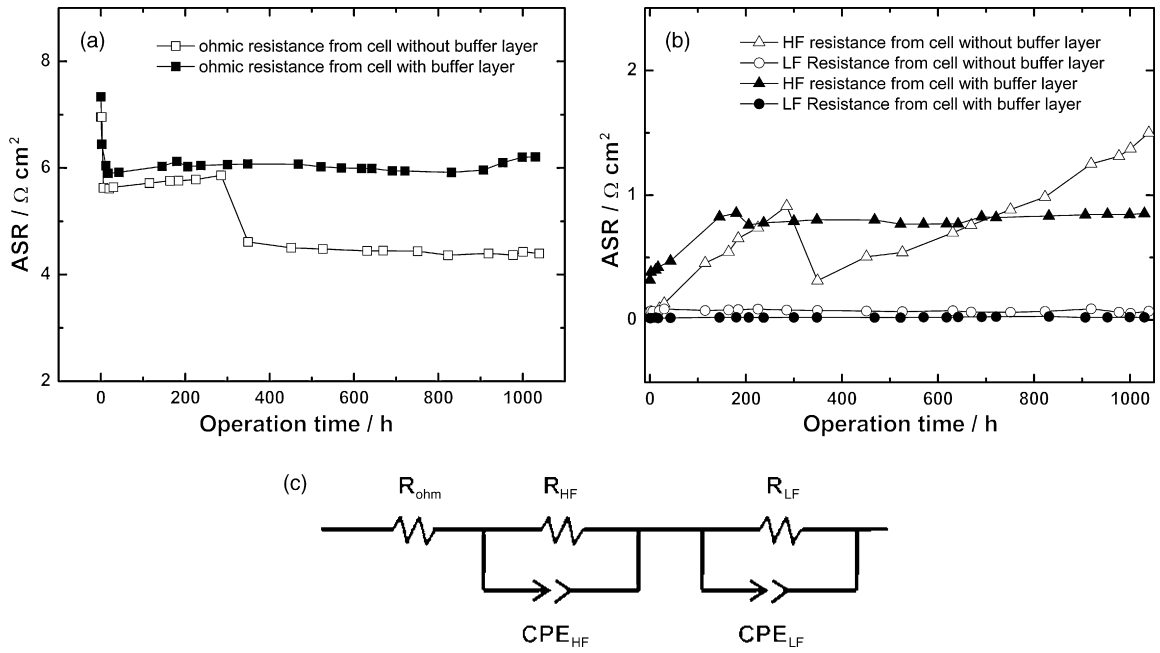


**Fig. 3.** Plot of ASR values obtained from impedance response of BSCF half-cells prepared in absence and presence of unsintered GDC buffer layers, as measured at 800 °C in ambient air for 1000 h: (a) ohmic resistance, (b) HF and LF impedance, and (c) equivalent circuit.

however, secondary phases are not detected after firing at 800 °C for 2 h. Zhu et al. [27] suggested that several undesired phases were detectable after heat treatment at 900 °C for 4 h. The results from this study indicate that at a relatively lower temperature of 800 °C, interactions between BSCF and YSZ can also occur during long-term operation (50 h) and lead to the formation of impure phases and a decay in SOFC performance.

### 3.2. Performance and durability of a symmetrical cell having an unsintered BSCF electrode with an unsintered GDC buffer layer situated between the BSCF and YSZ

To prevent interactions between the BSCF cathode and YSZ electrolyte, the use of GDC as a buffer layer is investigated. As mentioned previously, to overcome the problem involving fabrication of a metal-supported SOFC, an unsintered GDC buffer layer is needed. Unsintered BSCF symmetrical cells are fabricated in the presence and absence of an unsintered GDC buffer layer situated between the BSCF electrode and YSZ electrolyte. Fig. 3 shows how the impedance response develops with time in a cell having a GDC buffer layer (unsintered BSCF|unsintered GDC|YSZ|unsintered GDC|unsintered BSCF) and a cell without a GDC buffer layer (unsintered BSCF|YSZ|unsintered BSCF) while being exposed to ambient air at 800 °C for 1000 h. Ohmic resistances developed with time are shown in Fig. 3(a) and polarization resistances are presented in Fig. 3(b). The EIS response consists of two overlapping depressed arcs at high (HF) and low frequencies (LF), and it is fitted to an equivalent circuit using non-linear least squares fitting. The equivalent circuit is composed of a resistor in series with two parallel constant-phase element (CPE)–resistor combinations, as shown in Fig. 3(c).

Introducing an unsintered GDC buffer layer causes a relatively larger ohmic resistance and polarization resistance initially, but improves cell performance durability. The ASR with the cell having an unsintered buffer layer is more stable over 1000 h of operation compared with the cell having no buffer layer. There are, however, changes in the ohmic and polarization resistance of the cells in this study that are difficult to associate unequivocally with any particular mechanism without further study. The cell with a GDC buffer layer experiences a drop in ohmic resistance at 10 h and then remains constant, while the ohmic resistance decreases in two steps (at 10 h and at 300 h) in the cell without the GDC buffer layer. The former decrease in ohmic resistance within 10 h is probably caused by sintering between the Pt paste and Pt mesh current-collector, as this decrease occurs in both samples. The latter decrease in ohmic resistance together with HF resistance at 300 h in the non-buffered sample is unclear, as multiple phenomena can occur in this system. The HF resistance of the non-buffered cell dominates the total resistance and significantly increases, probably due to the formation of the secondary phases, while the LF resistance is fairly constant over 1000 h. Unexpectedly, the HF resistance of the buffered cell also increases during 0–200 h, similar to the non-buffered cell, and can arise from a change in the unsintered cathode microstructure. Later in this study, a large difference in performance between cells with sintered and unsintered cathodes is reported. After this initial increase, the HF resistance of the buffered cell remains constant over 800 h.

### 3.3. Comparison of performance and microstructure of SOFCs using sintered and unsintered GDC buffer layers

Given the performance durability of the half-cell using an unsintered GDC buffer layer, it is interesting to compare the performance of a single-cell using unsintered GDC with that of a cell using a sintered GDC layer. Anode-supported cells are used so that the buffer layer can be heat-treated in air. Therefore, anode-supported cells using an unsintered BSCF cathode, with a sintered GDC buffer layer or unsintered GDC buffer layer, were prepared.

The *I–V–P* curves of cells having sintered GDC buffer layers (Ni-YSZ/YSZ/sintered GDC/unsintered BSCF) and unsintered GDC buffer layers (Ni-YSZ/YSZ/unsintered GDC/unsintered BSCF) are presented in Fig. 4(a). Maximum power densities of 0.82 and 0.75 W cm$^{-2}$ are obtained from single-cells with sintered GDC and unsintered GDC buffer layers, respectively. The performance of the cell decreases slightly when unsintered GDC is used, having a performance difference of 0.07 W cm$^{-2}$. The maximum power density obtained from a single-cell using both a sintered BSCF cathode and

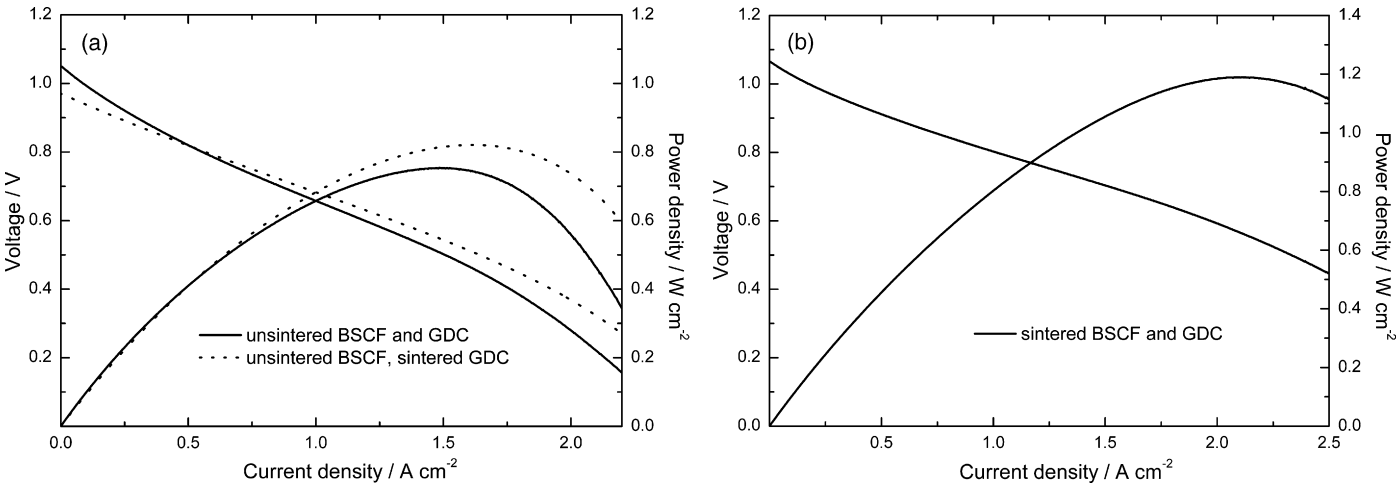


**Fig. 4.** *I–V–P* characteristics of anode-supported SOFCs showing (a) effect of unsintered GDC buffer layer (Ni-YSZ|YSZ|sintered GDC|unsintered BSCF in comparison with Ni-YSZ|YSZ|unsintered GDC|unsintered BSCF) and (b) base case (Ni-YSZ|YSZ|sintered GDC|sintered BSCF).

**Table 2**
Fitting results of impedance spectra obtained from a single-cell (Ni-YSZ|YSZ|unsintered GDC|unsintered BSCF) with respect to variation of thickness of GDC buffer layer, as measured at 800 °C (97% $H_2$ and 3% $H_2O$ at anode and ambient air at cathode).

| | Total polarization resistance ($\Omega\,cm^2$) | Ohmic resistance ($\Omega\,cm^2$) | HF resistance ($\Omega\,cm^2$) | LF resistance ($\Omega\,cm^2$) |
|---|---|---|---|---|
| 1T coating | 0.32 | 0.26 | 0.13 | 0.19 |
| 2T coating | 0.40 | 0.26 | 0.14 | 0.26 |
| 3T coating | 0.51 | 0.27 | 0.16 | 0.35 |

1T, 2T, 3T are one, two and three buffer layer coatings, respectively.

sintered GDC buffer layer was also measured as a base case, as shown in Fig. 4(b). A maximum power density of 1.23 W $cm^{-2}$ is achieved at 800 °C, and a large performance difference is clear in comparison with the cell using unsintered BSCF (the performance difference is 0.41 W $cm^{-2}$). These results indicate that the sintering process of the GDC buffer layer does not significantly influence the cell performance as much as the sintering process of the BSCF cathode, which largely increases cell performance.

It should be noted that the maximum power density obtained from the anode-supported cell having a GDC buffer layer is lower than that obtained from the anode-supported cell with no GDC buffer layer, which has been reported in previous work (0.91 W $cm^{-2}$) [17]. There are two reasons for this outcome. First, an *in situ* sintered BSCF cathode is used, so the non-buffered cell is exposed to a maximum temperature of 800 °C, which is the operating temperature used in this study. Therefore, after 2 h of operation when the measurement is made, there is no detrimental effect from the BSCF–YSZ interaction in the non-buffered cell. Second, introducing the buffer layer increases the ohmic resistance and may increase the interfacial resistance between the YSZ electrolyte and the GDC buffer layer. Although mixed ionic and electronic conductivity in the GDC layer can be expected to extend the three-phase boundary and lower the polarization resistance of the cell [24], the 1 μm-thick buffer layer examined in this study does not give such a benefit.

Photographs of the Ni-YSZ|YSZ|unsintered BSCF single-cell and the Ni-YSZ|YSZ|unsintered GDC|unsintered BSCF single-cell, after operation at 800 °C for 50 h, is shown in Fig. 5. In the case of Ni-YSZ|YSZ|unsintered BSCF, the BSCF cathode partly delaminates after operation, as can be seen in Fig. 5(a). This is probably caused by the large thermal expansion difference between the BSCF cathode and YSZ electrode. In the case of the Ni-YSZ|YSZ|unsintered GDC|unsintered BSCF single-cell, the GDC buffer layer improves the adhesion between the BSCF cathode and the cell. The BSCF cathode remains fused to the GDC buffer layer after operation, as shown in Fig. 5(b). The thermal expansion coefficients (TEC) of BSCF, GDC and YSZ are $24.3 \times 10^{-6}$ [28], $12 \times 10^{-6}$ [29] and $10.1 \times 10^{-6}\,K^{-1}$ [30], respectively.

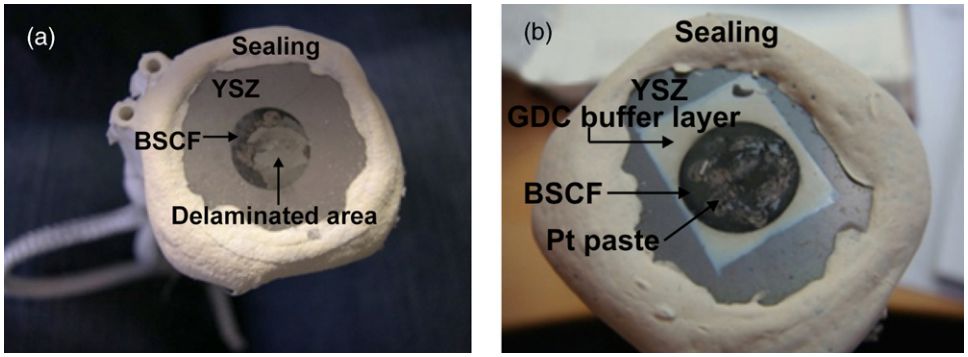


**Fig. 5.** Cell pictures of: (a) Ni-YSZ|YSZ|unsintered BSCF single-cell and (b) unsintered Ni-YSZ|YSZ|unsintered GDC|unsintered BSCF single-cell after operation at 800 °C for 20 h.

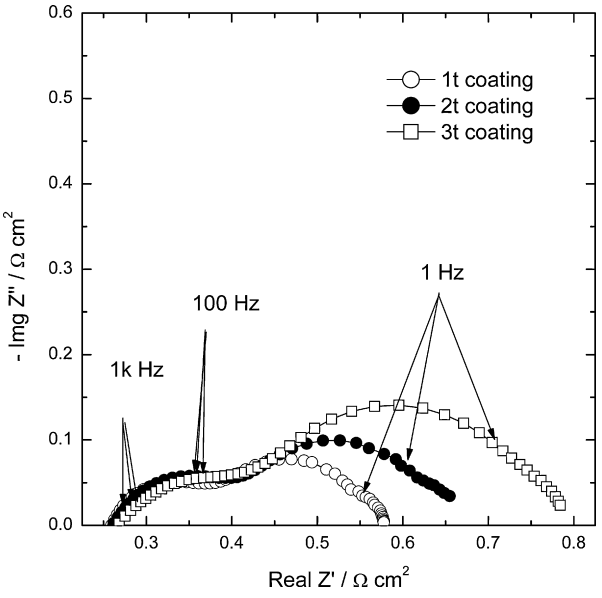


**Fig. 6.** Impedance spectra of single-cell (Ni-YSZ|YSZ|unsintered GDC|unsintered BSCF) with respect to variation of thickness of GDC buffer layer, as measured at 800 °C (97% $H_2$ and 3% $H_2O$ at anode and ambient air at cathode).

### 3.4. Effect of thickness of GDC buffer layer

Impedance spectra of a single-cell with respect to thickness of the GDC buffer layer, as measured at 800 °C (97% $H_2$ and 3% $H_2O$ at the anode, ambient air at the cathode), are presented in Fig. 6. The thickness of the layer is controlled by the number of coatings. It is evident that the EIS response consists of two overlapping

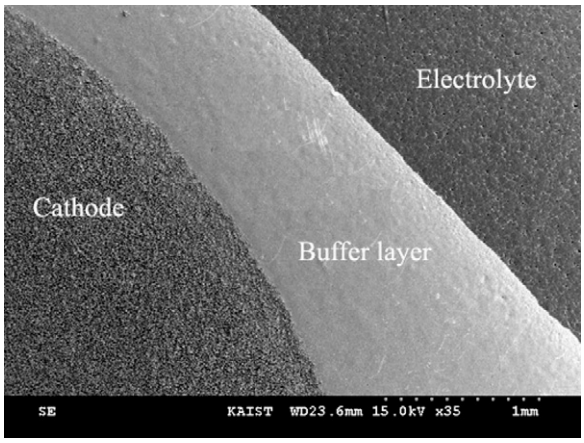


**Fig. 7.** SEM images observed from unsintered BSCF and unsintered GDC buffer layered single-cell (Ni-YSZ|YSZ|unsintered GDC|unsintered BSCF).

depressed arcs at HF and LF. The EIS response is again fitted to the equivalent circuit using a non-linear least squares procedure, as shown in Fig. 3(c). As depicted in Table 2, the ohmic resistance slightly increases with respect to the thickness of the buffer layer. As the thickness of buffer layer increases, the total polarization of the single-cell increases (0.32, 0.40 and 0.51 Ω $cm^2$, respectively). The thick GDC buffer layer can be considered as a resistance layer in this study. The LF resistance substantially increases compared with the HF resistance. The LF resistance in the buffered cell has been reported [24] to reflect the oxygen ion transfer resistance in porous thick GDC layers. Moreover, as shown below, the SEM images reveal delamination of the BSCF cathode in the cells having 2- and 3-times-coated GDC buffer layers, which can be one possible cause for the large increase in LF resistance observed in this study.

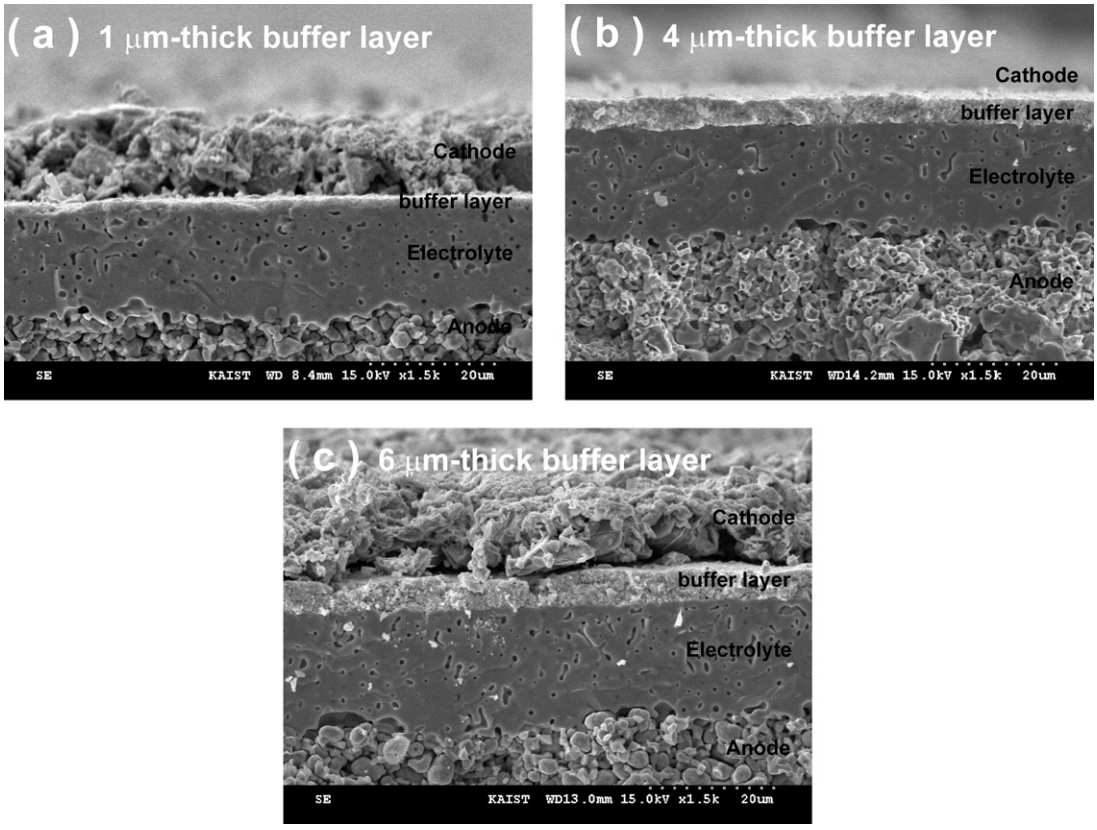


**Fig. 8.** Cross-sectional SEM images observed from cells with varied thicknesses of unsintered GDC buffer layer (Ni-YSZ|YSZ|unsintered GDC|unsintered BSCF).

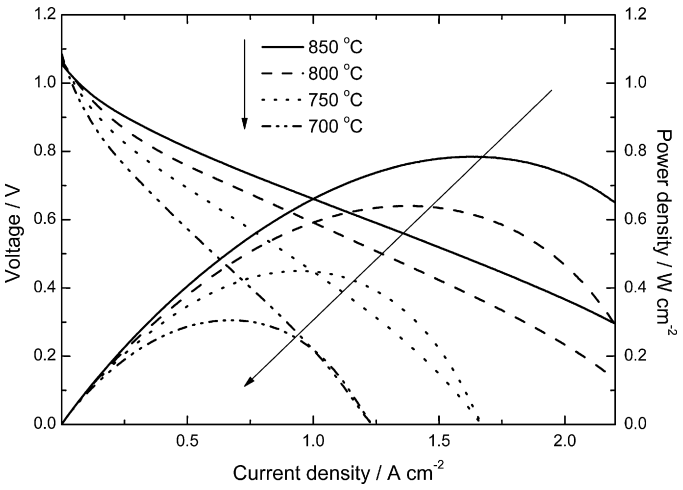


**Fig. 9.** *I–V–P* characteristics of metal-supported single-cell using unsintered BSCF cathode and unsintered GDC buffer layer (Ni-YSZ|YSZ|unsintered GDC|unsintered BSCF) as function of temperature.

The surface image of single-cells having an unsintered BSCF cathode and unsintered GDC buffer layer after SOFC operation is presented in Fig. 7. The cross-sectional SEM images of a single-cell with respect to the thickness of the unsintered GDC buffer layer are shown in Fig. 8. The images are taken from each cell after operation for 2 h at 800 °C (97% $H_2$ and 3% $H_2O$ to the anode and ambient air to the cathode). It is clear that although the buffer layer is not sintered at a high temperature, a dense GDC buffer layer is also formed when compared with the sintered YSZ electrolyte, which has a dense microstructure but contains closed pores. As shown in Fig. 8(a)–(c), the thicknesses of the GDC buffer layer in the prepared samples are ~1, 4 and 6 μm. The GDC layers remain dense and fused to the electrolyte as the thickness of the buffer layer is increased, which could indicate that *in situ* sintering during SOFC operation at 800 °C is sufficient to generate the dense structure of the GDC layer and cause adhesion of the layer to the electrolyte. It should be noted, however, that the GDC layer used in this study has a rather small particle size (0.5 μm), which can facilitate the *in situ* sintering of the GDC buffer layer.

In this study, the BSCF cathode adheres well to the GDC buffer layer in the case of the sample with a 1 μm-thick buffer layer, as shown in Fig. 8(a), while signs of delamination are evident in the sample with buffer layer thicknesses of 4 and 6 μm, as shown in Fig. 8(b) and (c), respectively. The reasons for the variation of delamination of the cathode with buffer layer thickness are unclear, but the thermal expansion mismatch between BSCF and GDC may dominate when a thick GDC buffer layer is used. It has been reported [31] that in the case of highly Co-doped cathode materials, a peeling-off phenomenon is observed due to the large TEC mismatch between BSCF and GDC. This phenomenon can also give rise to polarization and ohmic resistance in the cell. Therefore, a composite cathode of GDC and a BSCF cathode can be used to adjust the TEC [32]. The results indicate that if a proper thickness is used, the GDC buffer layer not only blocks the unwanted chemical reaction between the BSCF cathode and YSZ electrolyte, but also improves the unsintered BSCF cathode adhesion to the cell. The overly thick buffer layer causes delamination of the BSCF cathode.

### 3.5. Performance of metal-supported SOFC having an unsintered GDC buffer layer and unsintered BSCF at various operating temperatures

*I–V–P* curves are obtained from the metal-supported cell using an unsintered BSCF cathode and an unsintered GDC buffer layer at various temperatures, as shown in Fig. 9. The maximum power densities are 0.78, 0.64, 0.45 and 0.31 W $cm^{-2}$ at 850, 800, 750 and 700 °C, respectively. The OCV decreases with increasing temperature in accordance with the Nernst equation. In a similar fashion to the anode-supported cell, introducing a 1 μm-thick buffer layer decreases the cell performance in comparison with a cell without the buffer layer. The metal-supported cell in the presence of the GDC buffer layer exhibits a relatively lower maximum power density of 0.64 W $cm^{-2}$ at 800 °C compared with the cell in the absence of a buffer layer (0.81 W $cm^{-2}$) under the same operating conditions. Although fairly acceptable for metal-supported performance, the obtained performance is rather low relative to BSCF-based SOFCs. Optimization of the metal-supported cell fabrication is still required and is a subject of ongoing investigation.

## 4. Conclusions

The effect of an unsintered GDC buffer layer on the performance of SOFCs using an unsintered BSCF cathode is has been investigated. The cells are prepared in the presence and absence of GDC buffer layers. The cell performance durability is investigated. For the cells with a buffer layer, the performance and microstructure of the cells having sintered and unsintered GDC are studied, including the effect of buffer layer thickness.

Interaction between the unsintered BSCF cathode and YSZ electrolyte occurs at 800 °C during 50 h of operation, resulting in secondary phases that deteriorated cell performance durability. This is supported by the *I–V–P* characteristics and the XRD patterns. The *I–V–P* curve of the cell with no buffer layer shows a significant decay in cell performance after 50 h of operation, and XRD detects unwanted phases such as $SrZrO_3$ and $BaZrO_3$.

An unsintered GDC could be a promising option for use in metal-supported SOFC fabrication. After introducing an unsintered GDC buffer layer, the ASR of a cell having an unsintered buffer layer is relatively more stable over 1000 h of operation when compared with a cell having no buffer layer.

Comparable performance is obtained from cells having sintered and unsintered GDC buffer layers. The maximum power densities of the anode-supported cell using an unsintered BSCF cathode with a sintered GDC buffer layer and unsintered GDC buffer layer are 0.82 and 0.75 W $cm^{-2}$, respectively. Cell performance is significantly improved when a sintered BSCF cathode is used, with a maximum power density of 1.23 W $cm^{-2}$. The results indicate that the sintering process of the GDC buffer layer does not significantly influence the cell performance as much as the sintering process of the BSCF cathode.

In comparison with a cell with no buffer layer, adhesion of the BSCF cathode to a cell is enhanced by using a GDC buffer layer; however, the ASR of the cells increases as the buffer layer is introduced and an overly thick buffer layer also causes delamination of the BSCF cathode and thereby suggest that the thickness of the unsintered GDC buffer layer should be reduced.

The maximum power densities obtained from the metal-supported cells using unsintered BSCF and unsintered GDC buffer layers are 0.78, 0.64, 0.45 and 0.31 W $cm^{-2}$ at 850, 800, 750 and 700 °C, respectively.

## Acknowledgments

This work is the outcome of "the development program for Core Technologies for Fuel Cells (CTFC)" and "Solid oxide fuel cell of New & Renewable Energy R&D program (20093021030010)" of the Ministry of Knowledge Economy (MKE). Furthermore, this work was supported by "the Brain Korea 21 (BK21) program" and "The encouragement program for the EU FP participation" funded by the Ministry of Education, Science Technology (MEST).

## References


[1] R. O' Hayre, S.W. Cha, W. Colella, F.B. Prinz, Fuel Cell Fundamentals, Wiley, NY, USA, 2006.
[2] E. Fontell, T. Kivisaari, N. Christiansen, J.-B. Hansen, J. Pålsson, J. Power Sources 131 (2004) 49.
[3] Z.P. Shao, S.M. Haile, Nature 431 (2004) 170.
[4] C.-B. Lee, J.-M. Bae, J. Power Sources 176 (2008) 62.
[5] M.C. Tucker, C.P. Jacobson, L.C. De Jonghe, S.J. Visco, J. Power Sources 160 (2006) 1049.
[6] J.H. Joo, G.M. Choi, J. Power Sources 182 (2008) 589.
[7] R. Hui, J.O. Berghaus, C.D. -Petit, W. Qu, S. Yick, J.-G. Legoux, C. Moreau, J. Power Sources 191 (2009) 371.
[8] S.R. Hui, D. Yang, Z. Wang, S. Yick, C.D. -Petit, W. Qu, A. Tuck, R. Maric, D. Ghosh, J. Power Sources 167 (2007) 336.
[9] D. Stöver, D. Hathiramani, R. Vaßen, R.J. Damani, Surf. Coat. Technol. 201 (2006) 2002.
[10] S.J. Visco, C.P. Jacobson, I. Villareal, A. Leming, Y. Matus, L.C.D. Jonghe, Electrochem. Soc. Proc. 7 (2003) 1040.
[11] Y.B. Matus, L.C.D. Jonghe, C.P. Jacobson, S.J. Visco, Solid State Ionics 176 (2005) 443.
[12] M. Lang, T. Franco, R. Henne, S. Schaper, G. Schiller, Proceedings of the 4th European SOFC Forum, Lucerne, Switzerland, 2000, p. 231.
[13] G. Schiller, T. Franco, R. Henne, M. Lang, R. Ruckdäschel, Electrochem. Soc. Proc. 16 (2001) 885.
[14] G. Schiller, T. Franco, M. Lang, P. Metzger, A.O. Störmer, Electrochem. Soc. Proc. 7 (2005) 66.
[15] S.C. Singhal, K. Kendall, High Temperature Solid Oxide Fuel Cells: Fundamentals, Design and Application, Elsevier, Oxford, UK, 2003.
[16] M. Mori, T. Yamamoto, T. Ichikawa, Y. Takeda, Solid State Ionics 148 (2002) 93.
[17] Y.-M. Kim, P. Kim-Lohsoontorn, S.-W. Baek, J-M. Bae, in preparation.
[18] O. Yamamoto, Y. Takeda, R. Kanno, M. Noda, Solid State Ionics 22 (1987) 241.
[19] H.Y. Tu, Y. Takeda, N. Imanishi, O. Yamamoto, Solid State Ionics 117 (1999) 277.
[20] A.M. -Amesti, A. Larrañaga, L.M.R. -Martínez, A.T. Aguayo, J.L. Pizarro, M.L. Nó, A. Laresgoiti, M.I. Arriortua, J. Power Sources 185 (2008) 401.
[21] Y.D. Zhen, A.I.Y. Tok, S.P. Jiang, F.Y.C. Boey, J. Power Sources 178 (2008) 69.
[22] R. Hui, Z. Wang, O. Kesler, R. Maric, D. Ghosh, J. Power Sources 170 (2007) 308.
[23] R. Tian, J. Fan, Y. Liu, C. Xia, J. Power Sources 185 (2008) 1247.
[24] M. Yang, A. Yan, M. Zhang, Z. Hou, Y. Dong, M. Cheng, J. Power Sources 175 (2008) 345.
[25] A.D. Hawkes, D.J.L. Brett, N.P. Brandon, Int. J. Hydrogen Energy 34 (2009) 9558.
[26] Z. Duan, M. Yang, A. Yan, Z. Hou, Y. Dong, Y. Chong, M. Cheng, W. Yang, J. Power Sources 160 (2006) 57.
[27] Q. Zhu, T. Jin, Y. Yang, Solid State Ionics 177 (2006) 1199.
[28] B. Wei, Z. Lu, X. Huang, J. Miao, X. Sha, X. Xin, W. Su, J. Eur. Ceram. Soc. 26 (2006) 2827.
[29] H. Hayashi, M. Kanoh, C.J. Quan, H. Inaba, S. Wang, M. Dokiya, H. Tagawa, Solid State Ionics 132 (2000) 227.
[30] H. Hayasi, T. Saitou, N. Maruyama, H. Inaba, K. Kawamura, M. Mori, Solid State Ionics 176 (2005) 613.
[31] Y.H. Lim, J. Lee, J.S. Yoon, C.E. Kim, H.J. Hwang, J. Power Sources 171 (2007) 79.
[32] W.-X. Kao, M.-C. Lee, T.-N. Lin, C.-H. Wang, Y.-C. Chang, J. Power Sources 195 (2010) 2220.